Aberration Correction and Speckle Noise Reduction in Image Minified Lensless Holographic Projection Based on Digital Micro-Mirror Device

Xingjian Li, Bizhong Xia, Haibei Wang, and Ping Su, *Member, IEEE*

***Abstract*—Lensless holographic projection technology allows for removing of the projection lens and simplifies the optical projection system. It has great potential to be applied in the fields of three-dimensional printing, integrated circuit fabrication, and display. In this article, for image minified lensless holographic projection based on digital micro-mirror device (DMD), we examine the aberration that arises from the use of the DMD in the presence of oblique converging spherical wave illumination. To correct this aberration, we employ a diagonal compression technique on the target pattern. Additionally, we address the issue of speckle noise by relaxing the amplitude constraint in the non-signal domain, which is generated by our proposed aberration correction method. Importantly, this relaxation is achieved without reducing the size of the valid image. Our experimental results demonstrate the successful reconstruction of high-quality images in a lensless holographic projection system.**

***Index Terms*—Aberration correction, digital micro-mirror device, lensless holographic projection, speckle noise reduction, spherical wave illumination.**

I. Introduction

TRADITIONAL projection systems use lens groups or freeform mirrors to project patterns onto a screen. However, these systems are bulky, expensive, and have limitations in many applications. In recent years, there has been a growing interest in holographic projection due to its advantages of being compact, low-cost, and having high optical efficiency [1], [2], [3], [4]. A holographic projection system typically utilizes a spatial light modulator (SLM) that loads a computer-generated hologram (CGH). This CGH is then illuminated by a coherent light beam, and the resulting image is formed at a specific distance away through the process of diffraction after passing through the SLM. The need for lenses or freeform mirrors is eliminated in holographic projection [5], [6], [7]. Additionally, the reconstruction distance and image size can be adjusted in holographic projection. To generate the CGHs that are loaded onto the SLM, various techniques are employed, including non-iterative algorithms [8], [9] (such as direct binary search [9]), iterative algorithm (such as Gerchberg-Saxton algorithm [10], [11], two stage algorithm [12], error diffusion [13], region-based search method [14]), and deep learning models [15], [16], [17].

The most commonly used SLMs in holographic projection systems are liquid crystal on silicon (LCOS) devices [2], [7], [15] and digital micro-mirror devices (DMDs) [17], [18], [19], both of which are reflective elements. However, SLMs typically have strict requirements for incidence angles, which is impractical in projection devices. Oblique illumination beyond the requirements of the SLMs can cause aberrations. One possible solution to this problem is to add a prism before the SLM to correct the angle of incidence. However, this approach has drawbacks, such as increased light energy loss and increased complexity of the optical system. In holographic projection systems using LCOS, the astigmatism caused by oblique illumination can be corrected by adding a virtual cylindrical lens phase into the computer generated hologram (CGH) [20]. On the other hand, DMDs have several advantages over LCOS, including high frame rate(32 kHz) [21], a wide spectral range of operation (UV-IR), and high reliability, making them more suitable for many applications, including 3D-printing [22], [23], single-pixel imaging [24], [25], microscopy [26], [27], [28], spectroscopy [29], [30], pattern recognition [31], media analysis [32], etc. Some researchers have studied the projection system of DMD with spherical wave illumination [12], [17], but they have neglected the aberration. Some researchers have studied the aberrations generated by oblique plane wave incidents on DMDs [33] and have attempted to correct these aberrations by directly compressing holograms. However, compressing holograms can reduce the quality of the projected images. Some researchers have studied the aberration caused by the defects of DMD under plane wave illumination [34], [35], [36], but these theories can't correct the aberration caused by spherical illumination of DMD. In certain applications, such as large-field projection [17] and lithograph [37], spherical wave illumination is required to magnify or minify the projection pattern. However, oblique spherical waves introduce

Manuscript received 5 January 2024; accepted 10 January 2024. Date of publication 16 January 2024; date of current version 9 February 2024. This work was supported by the Shenzhen Key Basic Program under Grant JCYJ20200109143031287. *(Corresponding author: Ping Su.)*

Xingjian Li is with the Institute of Data and Information, Tsinghua Shenzhen International Graduate School, Tsinghua University, Shenzhen 518055, China, and also with the Beijing Institute of Space Mechanics and Electricity, Beijing 100094, China (e-mail: lixj20@tsinghua.org.cn).

Bizhong Xia, Haibei Wang, and Ping Su are with the Institute of Data and Information, Tsinghua Shenzhen International Graduate School, Tsinghua University, Shenzhen 518055, China (e-mail: xiabz@sz.tsinghua.edu.cn; hb-wang16@tsinghua.org.cn; su.ping@sz.tsinghua.edu.cn).

This article has supplementary downloadable material available at https://doi.org/10.1109/JPHOT.2024.3354556, provided by the authors.

Digital Object Identifier 10.1109/JPHOT.2024.3354556

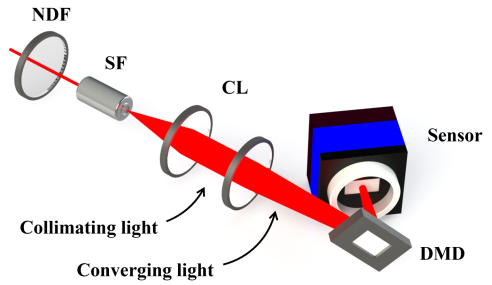

Fig. 1. Schematic of the proposed projection system. NDF, neutral density filter; SF, spatial filter; CL, convex lens; DMD, digital micromirror device.

more complex problems, and therefore new methods need to be developed to solve the aberration problem.

Severe speckle noise is often observed in the reconstructed hologram images obtained through iterative algorithms. This is primarily due to the fact that the amplitude or phase of a CGH is typically set to be completely uniform. As a result, it may be difficult or even impossible to find holograms that fully satisfy the constraints of both the projection plane and the holographic plane. In recent years, researchers have proposed methods to address this issue by combining amplitude constraints and introducing freedom in the image plane. One approach involves combining the amplitude of the target image with the amplitude of the previous iteration's reconstruction. This creates a new amplitude constraint on the target plane, which helps to avoid sharp intensity changes during the iteration process. By doing so, the iteration time is reduced and the overall quality of the reconstruction is improved [11], [38], [39]. Another method divides the image plane into two distinct regions: the signal domain and the non-signal domain. In this approach, the speckle noise is effectively reduced in the signal domain by ignoring the amplitude constraint in the non-signal domain [40], [41], [42], [43], [44]. However, it is important to note that the presence of the non-signal region leads to a reduction in the effective image pattern size.

This article presents a lensless holographic projection system based on DMD. The system aims to correct the aberration caused by oblique spherical wave illumination and suppress speckle noise in the signal domain, while maintaining the valid image pattern size. The optical layout of the proposed projection system is shown in Fig. 1. To address the aberration issue, the target pattern is compressed diagonally, resulting in the creation of extra pixels on the edge of the target image. These additional pixels naturally become the non-signal domain. By utilizing the amplitude freedom in the non-signal domain, the speckle noise in the target projection pattern, which is the signal domain, is effectively suppressed. This suppression of speckle noise leads to an improvement in the overall projection quality. At last, we demonstrate the effectiveness of the method by experiments.

The rest of this article is organized as follows. Section II analyzes the aberration caused by DMD illuminated by oblique converging spherical wave, and the formula for calculating and correcting aberrations is presented. In Section III, a method of amplitude constraint freedom in the non-signal domain is proposed to reduce the speckle noise of holographic projection.

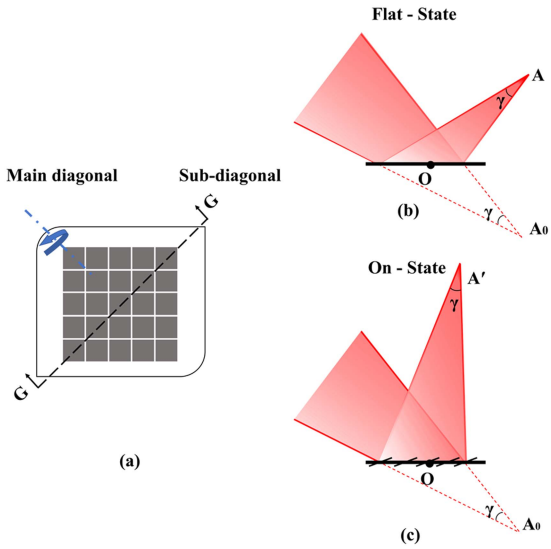

Fig. 2. Change of the focal length when oblique converging spherical wave reflected by the DMD. (a) Each micro-mirror is rotated around the axis in the main diagonal direction. (b) The oblique converging spherical wave is reflected by the DMD in the Flat-State, $OA = OA_0$. (c) The oblique converging spherical wave is modulated by the sub-diagonal direction of DMD in the On-State, $OA' > OA_0$.

Section IV presents and discusses the experimental results. Section V concludes the paper.

II. Aberration Correction

The DMD is composed of an array of micro-mirrors that rotate around the axis in the main diagonal direction, as depicted in Fig. 2(a). When the mirrors are not rotated, it is called the Flat-State; When the mirrors are rotated to the $+1$ direction (projection direction), it is called the On-State; When the mirrors are rotated to -1 direction, it is called the Off-State. Fig. 2(b) and (c) reveal the distinction between the Flat-State and the On-State of the DMD with spherical wave illumination. The convergence angle of the spherical wave is denoted as γ. When an oblique converging spherical wave illuminates the DMD in the Flat-State, the focal length of the spherical wave remains unchanged, denoted as $OA = OA_0$. However, when the same oblique converging spherical wave illuminates the DMD in the On-State in sub-diagonal direction, the focal length increases in the sub-diagonal direction due to the unique structure of the DMD [45]. This can be observed as $OA' > OA_0$.

As shown in Fig. 3, reflection in the main diagonal direction does not change the focal length, so the wave passes through the projection plane and still converges at point A. However, reflection in the sub-diagonal direction G-G results in an elongated focal length, which makes the incident wave converges at point A′, leading to aberration. This aberration is similar to astigmatism, as depicted as a deformed rectangle on the projection plane in Fig. 3(a). In our experiment, we observed a significant stretching of the projection pattern on the projection plane in the sub-diagonal direction G-G (P_1'– P_2' direction on the projection plane). To address this aberration, we conducted a

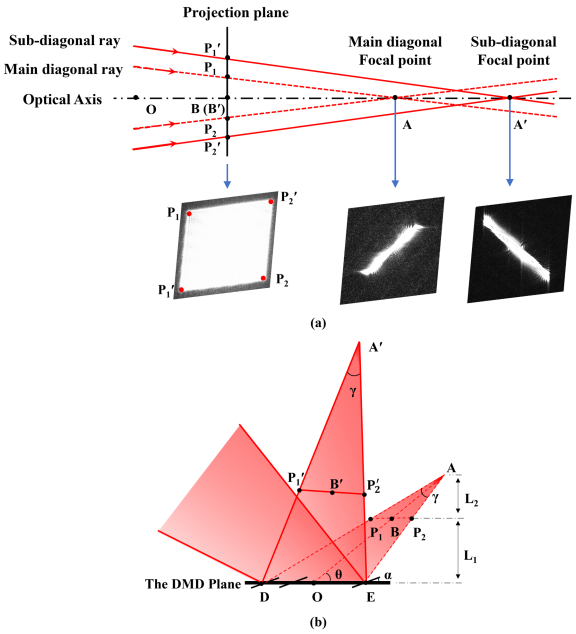

Fig. 3. Experiment and analysis of aberration caused by oblique converging spherical wave illuminated DMD. (a) Aberration in the experiment. The focal length becomes longer and the projection pattern is stretched in the sub-diagonal direction. (b) The rays with the DMD in the Flat-State are focused on point A; the rays with the DMD in the On-State are focused on point A′.

quantitative analysis and implemented corrective measures. See Visualization 1 for the aberration analysis experiment.

The angle at which the axis of the incident spherical wave intersects with the surface of the DMD is denoted as θ. The deflecting angle of the micro-mirrors is represented by α, while the convergence angle of the spherical wave is denoted as γ. In Fig. 3(b), it can be observed that the rays with the DMD in the Flat-State converge at point A, while the rays with the DMD in the On-State converge at point A′. Aberration occurs due to the fact that the wave in the sub-diagonal direction has different focal lengths with the DMD in the Flat-State and On-State. Consequently, the image on the projection plane exhibits different sizes in the main diagonal direction and the sub-diagonal direction with the DMD in the On-State, referred to as $L_{\text{main diagonal}}$ and $L_{\text{sub-diagonal}}$, respectively. This discrepancy in focal lengths leads to the stretching of the projection pattern along the sub-diagonal direction.

$$Aberration = \frac{Lmaindiagonal}{Lsub-diagonal} = \frac{P_1P_2}{P_1'P_2'} = \frac{\frac{L_2}{L_1+L_2}}{1-\frac{L_1}{A'O\sin\theta}} \tag{1}$$

In △A′DE, according to the sine theorem, we have:

$$\frac{DE}{\sin\gamma} = \frac{A'E}{\sin(\theta-\frac{\gamma}{2}+2\alpha)} = \frac{A'D}{\sin(\theta+\frac{\gamma}{2}+2\alpha)} \tag{2}$$

In the case of paraxial approximation, A′E∼A′D∼A′O≫DE, $\theta \gg \gamma$. (2) can be approximated as:

$$\left[\frac{DE}{\sin\gamma} = \frac{A'O}{\sin(\theta+2\alpha)}\right] \tag{3}$$

TABLE I
PARAMETERS OF THE COMPLETE OPTICAL PATH

Parameter	Value
The illumination wavelength, λ	639 nm
The pixel pitch of the DMD	7.56 μm
The resolution of the DMD	1080×1080
The deflecting angle of the micromirror, α	12°
Incidence angle, θ	45°
The distance between holographic plane midpoint O and the projection plane midpoint B, L_1	100 mm
The distance between the projection plane midpoint B and the focus point A, L_2	100 mm
Size of holographic plane	8.2×8.2 mm^2
Size of projection plane	4.1×4.1 mm^2

Also in △ADE, there is:

$$\frac{DE}{\sin\gamma} = \frac{AO}{\sin\theta} \tag{4}$$

Then (1) becomes:

$$Aberration = \frac{L_2}{L_2 + L_1(1-\frac{\sin\theta}{\sin(\theta+2\alpha)})} \tag{5}$$

Based on the analysis of (5), it can be deduced that when the angle θ is close to 90°, the value of sinθ changes at a slow rate. Consequently, if a spherical wave is incident vertically on the DMD plane (i.e., $\theta \sim 90°$), the value of sinθ can be approximated as sin(θ+2α), and the aberration is approximately equal to 1. As a result, aberration correction is not required in this scenario. However, if the incident wave is an oblique converging spherical wave, it becomes necessary to compress the target patterns along the sub-diagonal direction of the DMD. This compression operation effectively corrects the aberrations that occur after diffraction.

The parameters in the experiment are listed in Table I. By substituting the parameters into (5), it can be inferred that the projected pattern should be pre-compressed by 0.8 in the sub-diagonal direction.

The experimental results are presented in Fig. 4. It is evident that when a normal mesh is projected without pre-compression, the resulting pattern is distorted at an angle of 79.2°, which deviates by 10.8° from the true 90° angle. However, after compressing the pattern to 0.8 times its original size, as depicted in the second row of Fig. 4(a), the projected result exhibits minimal distortion with an angle of 89.5°. The angle error is reduced to 0.5°, which accounts for only 4.6% of the original error. The remaining aberration can be attributed to the limitations of the experimental equipment and the accuracy of the experimental alignment. Furthermore, the aberration correction experiment for the projection image "rabbit" is illustrated in Fig. 4(b). These results not only validate the effectiveness of (5), but also demonstrate that this method can effectively correct the aberration caused by the DMD with oblique converging spherical wave illumination.

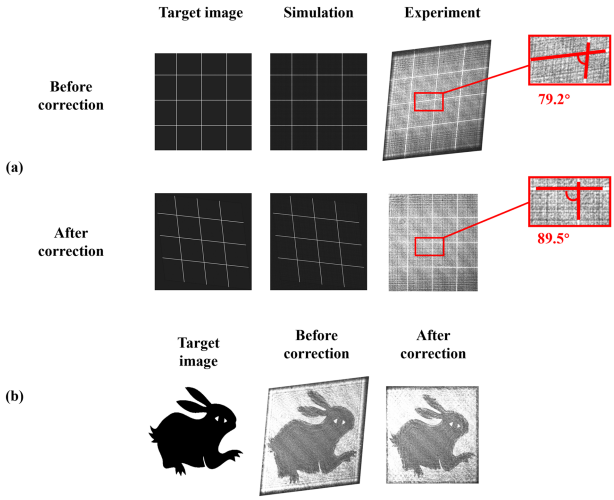

Fig. 4. Experiment of aberration correction. (a) Aberration correction of gridding and experimental verification. (b) Aberration correction experimental of image "rabbit".

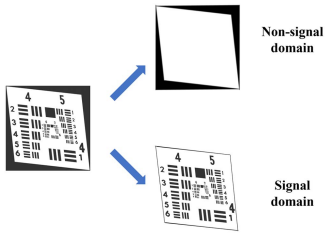

Fig. 5. Target pattern is divided into signal domain and non-signal domain.

III. Amplitude Constraint Freedom in the Non-Signal Domain

After pre-adjusting the target image for correction, the subsequent step involves calculating the CGH loaded onto the DMD plane. In the conventional GS algorithm, each iteration consists of a forward and a backward wavefront propagation between the image plane and the holographic plane. The wavefront propagation between these planes is typically described using the angular-spectrum method (ASM) [46]. In the ASM, the sampling points in both the image plane and the holographic plane are identical, as determined by the resolution of the SLM. However, if the image plane is divided into a signal domain and a non-signal domain, and the amplitude constraint is relaxed in the non-signal domain to suppress speckle noise, the field of view of the image will be reduced.

In Section II, the focal image undergoes compression along the diagonal axis as a corrective measure for aberration, consequently generating surplus pixels at the periphery of the focal image, as depicted in Fig. 5. The resolution of the full image is 1080×1080. The signal area is the target pattern compressed along the sub-diagonal, and the non-signal area is zero-padding in the lower left and upper right corners. The methodology we propose is illustrated in Fig. 6. Throughout the iterative process, the amplitude constraint within the non-signal domain is disregarded, thereby enhancing the quality of imaging within the signal domain. Subsequently, during the optical projection

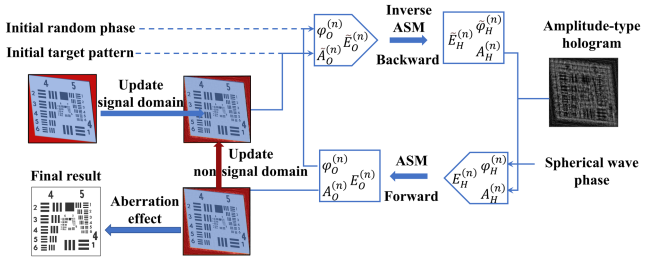

Fig. 6. Reduce speckle noise by relaxing amplitude constraint in the non-signal domain which generated by aberration correction.

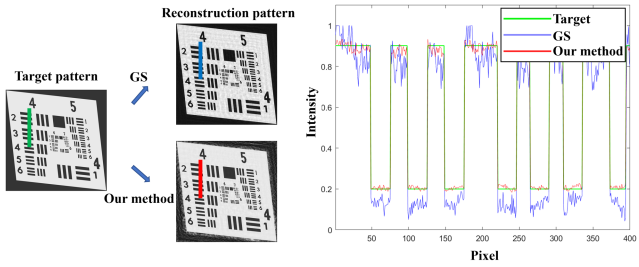

Fig. 7. Simulation results and reconstruction pattern quality comparison of GS method and the proposed method.

experiment, the aberration effect is tantamount to the expansion of the image pattern in the sub-diagonal direction. This approach effectively suppresses speckle noise and ensures that the field of view within the effective projection plane remains unaltered.

In an endeavor to efficiently regulate the noise within the non-signal domain, the aggregate energy within the holographic plane is meticulously managed to match the energy of the target reconstructed pattern. This approach is predicated on the principle of energy conservation [41].

$$\iint \left|E_O(x,y)\right|^2 dxdy = \iint \left|E_H(u,v)\right|^2 dudv \tag{6}$$

$|E_O(x,y)|^2$denotes the energy associated with the target reconstruction pattern, while $|E_H(u,v)|^2$ signifies the energy inherent in the hologram. In the context of an amplitude-type hologram, it is possible to proportionally adjust the amplitude of every pixel within the hologram. This adjustment aims to equate the energy present on the holographic plane with the energy of the target reconstruction pattern.

The parameters of simulation there are the same as those used in Section II. The depth of the amplitude Fresnel hologram is 8 bits. As a rule of thumb, we chose the iteration number 200. The Amplitude-type SLM is not suitable for holographic reconstruction of patterns with very high contrast. In order not to introduce additional errors, we adjusted the maximum and minimum intensity of the target image to 0.9 and 0.2. Using the compressed USAF 1951 test chart pattern as a representative example, we computed the corresponding CGH via both the proposed method and the GS algorithm. The reconstruction outcomes of the two CGHs are visually represented in Fig. 7. Upon comparison with the result obtained through the GS algorithm, it is evident that speckle noise is efficaciously mitigated in the outcome derived from the proposed method. Furthermore, the

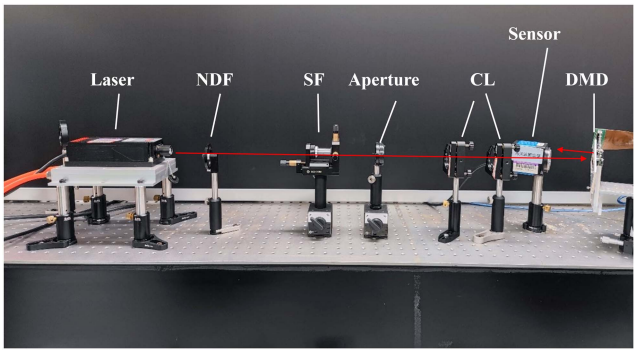

Fig. 8. Experimental setup of the holographic projection system. NDF, neutral density filter; SF, spatial filter; CL, convex lens; DMD, digital mirror device.

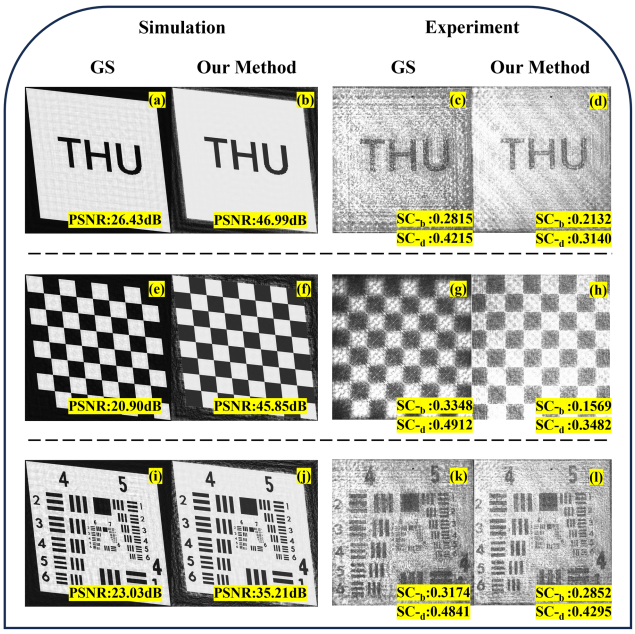

Fig. 9. Holographic reconstruction and experimental verification of alphabet "THU", checkerboard and USAF 1951 test chart. (a), (b), (e), (f), (i), (j) are the simulation reconstruction images of the GS algorithm and our method. (c), (d), (g), (h), (k), (l) are the optical reconstruction images of the GS algorithm and our method. The peak signal-to-noise ratio (PSNR) and the speckle contrast (SC) is used to analysis simulation and experiment results.

peak signal-to-noise ratio (PSNR) in the signal domain of the reconstruction results experienced a significant increase from 23.03 dB (as achieved by the GS algorithm) to 35.21 dB (as achieved by the proposed method).

IV. Experiments

The experimental configuration for the image minification through lensless holographic projection, utilizing a DMD, is depicted in Fig. 8. The laser beam, after traversing a neutral density filter and a spatial filter, is transformed into a converging spherical wave by the convex lens. Subsequently, this spherical wave undergoes modulation by a DMD (specifically, a DLP6500 model) and is projected onto an image sensor (PCO Panda26 model). The parameters employed in this experimental setup mirror those used in the numerical simulation.

The experiment results are presented in Fig. 9. The quality of the simulation-reconstructed images was assessed using the PSNR. Additionally, the speckle contrast (SC) was employed to quantify the blurring of the speckle noise in the optically reconstructed images. The SC is defined as the ratio of the standard deviation to the mean value of the reconstruction image. SC-$_{\mathrm{b}}$ means the SC in bright-region and SC-$_{\mathrm{d}}$ means the SC in dark-region. The lower SC indicates the reduction in the occurrence of speckle noise in the optically reconstructed image.

The experimental images are obtained under the same camera exposure time. Part of the reason why the experimental results of our method are enhanced in brightness comes from the fact that the target patterns in our method are surrounded by the non-signal domain, so the middle part of the hologram can use a higher "transmittance" in the hologram calculation process without worrying about diffracting into the surrounding non-signal domain.

The experimental results provide robust validation of the efficacy of the aberration correction formula (5) and the proposed method. The projection aberration is effectively rectified, and the speckle noise is significantly suppressed.

V. Conclusion

In this article, we introduce a novel formula designed to calculate the aberration of a converging spherical wave that illuminates a DMD. This aberration is subsequently eliminated through the strategic diagonal scaling of the target image. The target image undergoes a process of diagonal compression, which consequently leads to the generation of surplus pixels along the periphery of the said image. These extra pixels inherently transform into the non-signal domain. Following this, we propose an innovative method that relaxes the amplitude constraint within the non-signal domain, which is generated as a result of the aberration correction. This method effectively suppresses the inherent speckle noise in holographic projection, without necessitating a reduction in the size of the valid projection image. This is primarily due to the fact that the non-signal domain does not encompass any pertinent information about the intended target image.

In the final phase of our study, we design a lensless holographic projection system that is minified in scale and based on the DMD. Both simulation and experimental results demonstrate that this system is capable of achieving high-quality holographic projection.

Furthermore, the proposed projection system can be seamlessly integrated into various applications, including but not limited to lithography and 3D-printing. For lithography, the manufacturing time of a single-layer mask is about 2-10 hours [47], [48], while generating a hologram (200 iterations in our experiments) only takes 1 minute with the projection accuracy of approximately 10 μm. Additionally, the holographic projection is compact, allowing for removing of the projection lens and easy adjustment of the projection distance by changing the diffraction distance. As for 3D-printing, it's possible that the DMD can be loaded with 3D holograms and realizing processing on inclined

planes or 3D surfaces. This feature combines high efficiency with better adaptability to different surface profiles.

REFERENCES

[1] K. Wakunami et al., "Projection-type see-through holographic three-dimensional display," *Nature Commun.*, vol. 7, Oct. 2016, Art. no. 12954.

[2] E. Buckley, "Holographic laser projection," *J. Display Technol.*, vol. 7, no. 3, pp. 135–140, Mar. 2011.

[3] T. Takahashi, T. Shimobaba, T. Kakue, and T. Ito, "Time-division color holographic projection in large size using a digital micromirror device," *Appl. Sci.*, vol. 11, no. 14, Jul. 2021, Art. no. 6277.

[4] S.-T. Yu, A. Luo, L. Jiang, Y.-F. Liu, L. Gong, and Z.-S. Yuan, "Direct binary search method for high-resolution holographic image projection," *Opt. Exp.*, vol. 30, no. 15, pp. 26856–26864, Jul. 2022.

[5] F. C. Zhang, I. Yamaguchi, and L. P. Yaroslavsky, "Algorithm for reconstruction of digital holograms with adjustable magnification," *Opt. Lett.*, vol. 29, no. 14, pp. 1668–1670, Jul. 2004.

[6] W. D. Qu, H. R. Gu, H. Zhang, and Q. F. Tan, "Image magnification in lensless holographic projection using double-sampling Fresnel diffraction," *Appl. Opt.*, vol. 54, no. 34, pp. 10018–10021, Dec. 2015.

[7] C. L. Chang, Y. J. Qi, J. Wu, J. Xia, and S. P. Nie, "Image magnified lensless holographic projection by convergent spherical beam illumination," *Chin. Opt. Lett.*, vol. 16, no. 10, Oct. 2018, Art. no. 100901.

[8] L. Z. Chen, H. Zhang, L. C. Cao, and G. F. Jin, "Non-iterative phase hologram generation with optimized phase modulation," *Opt. Exp.*, vol. 28, no. 8, pp. 11380–11392, Apr. 2020.

[9] J.-H. Kang, T. Leportier, M. Kim, and M.-C. Park, "Non-iterative direct binary search algorithm for fast generation of binary holograms," *Opt. Lasers Eng.*, vol. 122, pp. 312–318, Nov. 2019.

[10] R. W. Gerchberg and W. O. Saxton, "Practical algorithm for determination of phase from image and diffraction plane pictures," *Optik*, vol. 35, no. 2, pp. 237–245, 1972.

[11] J. R. Fienup, "Iterative method applied to image-reconstruction and to computer-generated holograms," *Opt. Eng.*, vol. 19, no. 3, pp. 297–305, 1980.

[12] P. A. Cheremkhin, N. N. Evtikhiev, V. V. Krasnov, R. S. Starikov, and E. Y. Zlokazov, "Iterative synthesis of binary inline fresnel holograms for high-quality reconstruction in divergent beams with DMD," *Opt. Lasers Eng.*, vol. 150, Mar. 2022, Art. no. 106859.

[13] G. Yang, S. Jiao, J.-P. Liu, T. Lei, and X. Yuan, "Error diffusion method with optimized weighting coefficients for binary hologram generation," *Appl. Opt.*, vol. 58, no. 20, pp. 5547–5555, Jul. 2019.

[14] C. Lu et al., "A region based random multi-pixel search algorithm to improve the binary hologram reconstruction quality," *Opt. Lasers Eng.*, vol. 161, Feb. 2023, Art. no. 107322.

[15] L. Shi, B. C. Li, C. Kim, P. Kellnhofer, and W. Matusik, "Towards real-time photorealistic 3D holography with deep neural networks," *Nature*, vol. 591, no. 7849, pp. 234–238, Mar. 2021.

[16] J. C. Wu, K. X. Liu, X. M. Sui, and L. C. Cao, "High-speed computer-generated holography using an autoencoder-based deep neural network," *Opt. Lett.*, vol. 46, no. 12, pp. 2908–2911, Jun. 2021.

[17] P. Su, J. R. Wang, C. Cai, J. S. Ma, and Q. F. Tan, "Large field-of-view lensless holographic dynamic projection system with uniform illumination and U-net acceleration," *Opt. Lasers Eng.*, vol. 156, Sep. 2022, Art. no. 107106.

[18] T. Kreis, P. Aswendt, and R. Höfling, "Hologram reconstruction using a digital micromirror device," *Opt. Eng.*, vol. 40, no. 6, pp. 926–933, Jun. 2001.

[19] J.-Y. Son, B.-R. Lee, O. O. Chernyshov, K.-A. Moon, and H. Lee, "Holographic display based on a spatial DMD array," *Opt. Lett.*, vol. 38, no. 16, pp. 3173–3176, Aug. 2013.

[20] J. Starobrat, P. Wilczynska, and M. Makowski, "Aberration-corrected holographic projection on a two-dimensionally highly tilted spatial light modulator," *Opt. Exp.*, vol. 27, no. 14, pp. 19270–19281, Jul. 2019.

[21] D. Chen, S. Gu, and S.-C. Chen, "Study of optical modulation based on binary masks with finite pixels," *Opt. Lasers Eng.*, vol. 142, Jul. 2021, Art. no. 106604.

[22] H. Kadry, S. Wadnap, C. Xu, and F. Ahsan, "Digital light processing (DLP) 3D-printing technology and photoreactive polymers in fabrication of modified-release tablets," *Eur. J. Pharmaceut. Sci.*, vol. 135, pp. 60–67, Jul. 2019.

[23] W. Ouyang, X. Xu, W. Lu, N. Zhao, F. Han, and S.-C. Chen, "Ultrafast 3D nanofabrication via digital holography," *Nature Commun.*, vol. 14, no. 1, pp. 1716–1716, Mar. 2023.

[24] M. F. Duarte et al., "Single-pixel imaging via compressive sampling," *IEEE Signal Process. Mag.*, vol. 25, no. 2, pp. 83–91, Mar. 2008.

[25] Z. Zhang, S. Liu, J. Peng, M. Yao, G. Zheng, and J. Zhong, "Simultaneous spatial, spectral, and 3D compressive imaging via efficient Fourier single-pixel measurements," *Optica*, vol. 5, no. 3, pp. 315–319, Mar. 2018.

[26] M. H. Liang, R. L. Stehr, and A. W. Krause, "Confocal pattern period in multiple-aperture confocal imaging systems with coherent illumination," *Opt. Lett.*, vol. 22, no. 11, pp. 751–753, Jun. 1997.

[27] F. P. Martial and N. A. Hartell, "Programmable illumination and high-speed, multi-wavelength, confocal microscopy using a digital micromirror," *PLoS One*, vol. 7, no. 8, Aug. 2012, Art. no. 2365.

[28] J. Cheng, C. Gu, D. Zhang, D. Wang, and S.-C. Chen, "Ultrafast axial scanning for two-photon microscopy via a digital micromirror device and binary holography," *Opt. Lett.*, vol. 41, no. 7, pp. 1451–1454, Apr. 2016.

[29] Y. Wu, I. O. Mirza, G. R. Arce, and D. W. Prather, "Development of a digital-micromirror-device-based multishot snapshot spectral imaging system," *Opt. Lett.*, vol. 36, no. 14, pp. 2692–2694, Jul. 2011.

[30] Z. Liao, F. Sinjab, G. Gibson, M. Padgett, and I. Notingher, "DMD-based software-configurable spatially-offset raman spectroscopy for spectral depth-profiling of optically turbid samples," *Opt. Exp.*, vol. 24, no. 12, pp. 12701–12712, Jun. 2016.

[31] P. A. Cheremkhin, V. V. Krasnov, V. G. Rodin, and R. S. Starikov, "DMD-based optical pattern recognition using holograms generated with the Hartley transform," *Opt. Lasers Eng.*, vol. 166, Jul. 2023, Art. no. 107584.

[32] D. B. Conkey, A. M. Caravaca-Aguirre, and R. Piestun, "High-speed scattering medium characterization with application to focusing light through turbid media," *Opt. Exp.*, vol. 20, no. 2, pp. 1733–1740, Jan. 2012.

[33] D. M. Benton, "Multiple beam steering using dynamic zone plates on a micromirror array," *Opt. Eng.*, vol. 57, no. 7, Jul. 2018, Art. no. 073109.

[34] J. Hu, X. Xie, and Y. Shen, "Quantitative phase imaging based on wavefront correction of a digital micromirror device," *Opt. Lett.*, vol. 45, no. 18, pp. 5036–5039, Sep. 2020.

[35] J. Gene, J. M. Sohn, H. C. Shin, and S. Park, "Defect corrections for coherent optical information processing of grayscale images in a DMD-based 4f-system using a collimated light source," *Opt. Exp.*, vol. 30, no. 21, pp. 38821–38831, Oct. 2022.

[36] D. Benton, "Aberration and coherence effects with a micromirror array," in *Proc. SPIE. Int. Soc. Opt. Eng.*, 2021, pp. 13–17.

[37] R. Chen et al., "Edge smoothness enhancement in DMD scanning lithography system based on a wobulation technique," *Opt. Exp.*, vol. 25, no. 18, pp. 21958–21968, Sep. 2017.

[38] R. Di Leonardo, F. Ianni, and G. Ruocco, "Computer generation of optimal holograms for optical trap arrays," *Opt. Exp.*, vol. 15, no. 4, pp. 1913–1922, Feb. 2007.

[39] S. P. Poland, N. Krstajic, R. D. Knight, R. K. Henderson, and S. M. Ameer-Beg, "Development of a doubly weighted gerchberg-saxton algorithm for use in multibeam imaging applications," *Opt. Lett.*, vol. 39, no. 8, pp. 2431–2434, Apr. 2014.

[40] K. X. Liu, Z. H. He, and L. C. Cao, "Double amplitude freedom Gerchberg-Saxton algorithm for generation of phase-only hologram with speckle suppression," *Appl. Phys. Lett.*, vol. 120, no. 6, Feb. 2022, Art. no. 061103.

[41] L. Z. Chen, S. Z. Tian, H. Zhang, L. C. Cao, and G. F. Jin, "Phase hologram optimization with bandwidth constraint strategy for speckle-free optical reconstruction," *Opt. Exp.*, vol. 29, no. 8, pp. 11645–11663, Apr. 2021.

[42] C. L. Chang, J. Xia, L. Yang, W. Lei, Z. M. Yang, and J. H. Chen, "Speckle-suppressed phase-only holographic three-dimensional display based on double-constraint Gerchberg-Saxton algorithm," *Appl. Opt.*, vol. 54, no. 23, pp. 6994–7001, Aug. 2015.

[43] H. Akahori, "Spectrum leveling by an iterative algorithm with a dummy area for synthesizing the kinoform," *Appl. Opt.*, vol. 25, no. 5, pp. 802–811, Mar. 1986.

[44] B. B. Chhetri, S. Y. Yang, and T. Shimomura, "Iterative stepwise binarization of digital amplitude holograms with added energy to the signal window," *Opt. Eng.*, vol. 40, no. 12, pp. 2718–2725, Dec. 2001.

[45] C. Gong and D. Mehrl, "Characterization of the Digital Micromirror Devices," *IEEE Trans. Electron Devices*, vol. 61, no. 12, pp. 4210–4215, Dec. 2014.

[46] J. W. Goodman, *Introduction to Fourier optics*, 4th ed., New York, NY, USA: McGraw-Hill, 2017, pp. 61–66.

[47] A. Fujimura and J. Willis, "2019 mask makers' survey conducted by the eBeam Initiative," in *Proc. SPIE. Int. Soc. Opt. Eng.*, 2018, pp. 16–18.

[48] J. Heo, H. Min, and M. Lee, "Laser micromachining of permalloy for fine metal mask," *Int. J. Precis. Eng. Manuf.*, vol. 2, no. 3, pp. 225–230, Jul. 2015.